UC Merced
UC Merced Previously Published Works

Title
Colloids in confined liquid crystals: a plot twist in the lock-and-key mechanism

Permalink
https://escholarship.org/uc/item/90b8x9z5

Journal
Soft Matter, 15(26)

ISSN
1744-683X

Authors
Boniello, Giuseppe
Luo, Yimin
Beller, Daniel A
et al.

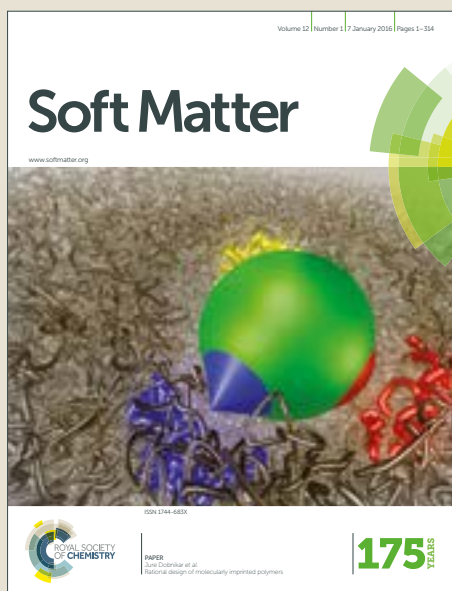**Publication Date**
2019-07-14

DOI
10.1039/c9sm00788a

Peer reviewed

Soft Matter

Accepted Manuscript

Volume 12 | Number 1 | 7 January 2016 | Pages 1–314

Soft Matter

www.softmatter.org

ISSN 1744-683X

ROYAL SOCIETY
OF CHEMISTRY

PAPER
Jure Dobnikar et al.
Rational design of molecularly imprinted polymers

175 YEARS

This is an Accepted Manuscript, which has been through the Royal Society of Chemistry peer review process and has been accepted for publication.

Accepted Manuscripts are published online shortly after acceptance, before technical editing, formatting and proof reading. Using this free service, authors can make their results available to the community, in citable form, before we publish the edited article. We will replace this Accepted Manuscript with the edited and formatted Advance Article as soon as it is available.

You can find more information about Accepted Manuscripts in the author guidelines.

Please note that technical editing may introduce minor changes to the text and/or graphics, which may alter content. The journal's standard Terms & Conditions and the ethical guidelines, outlined in our author and reviewer resource centre, still apply. In no event shall the Royal Society of Chemistry be held responsible for any errors or omissions in this Accepted Manuscript or any consequences arising from the use of any information it contains.

ROYAL SOCIETY
OF CHEMISTRY

rsc.li/soft-matter-journal

Journal Name

ARTICLE TYPE

Colloids in confined liquid crystals: a plot twist in the lock-and-key mechanism †

Giuseppe Boniello,[a] Yimin Luo,[a] Daniel A. Beller,[b] Francesca Serra,[*c] Kathleen J. Stebe[*a]

By confining soft materials within tailored boundaries it is possible to design energy landscapes to address and control colloidal dynamics. This provides unique opportunities to create reconfigurable, hierarchically organized structures, a leading challenge in materials science. Example soft matter systems include liquid crystals. For instance, when nematic liquid crystals (NLCs) are confined in a vessel with undulated boundaries, bend and splay distortions can be used to position particles. Here we confine this system in a twist cell. We also study cholesteric liquid crystals, which have an "intrinsic" twist distortion which adds to the ones imposed by the solid boundaries. The cholesteric pitch competes with the other length scales in the system (colloid radius, vessel thickness, wavelength of boundaries undulations), enriching the possible configurations. Depending on the pitch-to-radius and pitch-to-thickness ratios the interaction can be attractive or repulsive. By tuning the pitch (i.e. changing the concentration of the chiral dopant), it is possible to selectively promote or inhibit particle trapping at the docking sites.

1 Introduction

Bottom-up assembly of colloidal particles can be employed to efficiently build hierarchically ordered structures[1–3], such as photonic crystals[4,5], self-healing materials[6,7] or sensors[8,9]. Even more interesting are reconfigurable structures, where particles configuration and/or order (and, with them, optical and mechanical properties) change under the effect of external inputs, e.g. temperature, magnetic or electrical fields, chemical composition[10–12]. The ability to address the dynamics and localize single particles is crucial for these goals. Complex fluids such as liquid crystals are perfect tools to gain control over the motion of colloidal building blocks[13,14]. Liquid crystals have a dual nature. As fluids, they provide a perfect environment for colloidal motion. As crystals, they can store elastic energy when molecular orientational order deviates from the equilibrium configuration. For small deformations, the Frank-Oseen free energy density is written[15,16]:

$$f = \frac{1}{2}K_1(\nabla \cdot \hat{\mathbf{n}})^2 + \frac{1}{2}K_2(\hat{\mathbf{n}} \cdot \nabla \times \hat{\mathbf{n}} - q_0)^2 + \frac{1}{2}K_3(\hat{\mathbf{n}} \times \nabla \times \hat{\mathbf{n}})^2$$

where the director $\hat{\mathbf{n}}$, a headless vector, gives the local mean molecular orientation, and K_1, K_2, K_3 are the elastic constants associated to splay, twist and bend distortions, respectively. The helical wave number q_0 takes into account intrinsic twist distortion in the case of cholesteric LCs. Strong anchoring at the particle surface contributes to the creation of defects and distortions and topological defects[17]. Given their high energetic cost, particles tend to share defects forming linear, 2-dimensional or 3-dimensional aggregates[18,19], such as wires or sheets[20,21]. Confinement provides additional opportunities to drive colloidal behavior in liquid crystals. Vessel boundaries can be used to mold the energy landscape by introducing controlled or adjustable anchoring conditions to dictate director field distortions[22–24]. Curved boundaries, corners and protrusions act as attractive or repulsive sites for colloidal particles in LCs, and thus they create elastic energy gradients that determine the colloids' trajectories and interactions[25–29]. Recently, we have applied these principles to spherical homeotropic particles in quasi 2-D geometry in proximity to a wavy wall[30,31]. The waviness of the wall introduces sites of high splay energy density at the convex hills and in the concave dales, and sites of high bend energy density at the inflection points. These distortions couple with the complementary ones around the colloids. As a result, the particles dock at the

[a] Chemical and Biomolecular Engineering, University of Pennsylvania, Philadelphia, PA, 19104, USA. Fax: +1-(215)573-2093; Tel: +1-(215)898-8351; E-mail: kstebe@seas.upenn.edu

[b] Department of Physics, University of California, Merced, CA 95343, USA.

[c] Physics and Astronomy, Johns Hopkins University, Baltimore, MD, 21218, USA. Tel: +1-(410) 516-0248; E-mail: fserra1@jhu.edu

† Electronic Supplementary Information (ESI) available. See DOI: 00.0000/00000000.

wall.

Here, we introduce a "twist in the plot" by imposing a twist distortion in the same experimental setup. From a fundamental point of view, this new configuration allows us to explore all the principal modes of deformation of liquid crystals, i.e. splay, twist and bend. The director field, and the energy landscape with it, is molded in three dimensions, as it now depends on the vertical coordinate as well. From a practical perspective, twist provides a high degree of manipulability of the system. Twist distortions can be easily introduced, tuned and controlled in our sample. For smaller deformations, it is sufficient to use tilted anchoring directions in the boundaries to twist nematic LCs. For arbitrary twist, cholesteric LCs show an intrinsic twist distortion, given by chiral doping. In both cases the twist distortion is associated with a characteristic length scale, the pitch, i.e. the distance over which the director does a full rotation. The pitch couples and competes with all the other lengths in the system, in particular the cell thickness and the particle size, enriching the possibilities for lock-and-key interactions. Moreover, twist distortions can be dynamically adjustable by external parameters: temperature[32,33], chiral dopant concentration[34,35], boundaries alignment[36,37].

2 Experimental and numerical methods

The experimental setup is designed in order to guarantee a strong confinement to the LC phase within thin cells and to introduce controlled distortions via a wavy wall. Furthermore, by rotating the top plate, the setup induces director twist in nematic LCs, or accommodates it in cholesteric LCs. As described in our previous work[30] the cell is delimited by two parallel glass slides (Fig. 1). Glass slides have been previously spin-coated with $1wt\%$ PVA (poly(vinyl alcohol)) in DI water (20 s at 2000 rpm) or polyimide (40 s at 4000 rpm), annealed for an hour at $80°C$ and rubbed with a velvet cloth to ensure an uniform planar anchoring along rubbing direction. The top glass slide is in-plane rotated by an angle θ. The cell contains a wavy wall, which acts as a vertical boundary and as a spacer. The wall is made by photolithography with SU-8 (MicroChem Corp.), coated with silica by chemical vapor deposition and treated by immersion (8-10 min) in $3wt\%$ DMOAP (dimethyloctadecyl(3-(trimethoxysilyl)propyl)) (Sigma-Aldrich). The latter imposes a strong homeotropic or perpendicular anchoring on the wall. The wall thickness is 25μm. The radius of curvature of both wall's hills and dales are comparable to the particle radius. Once the cell is prepared in a "sandwich" configuration, the sample is sealed with optical glue (Norland Optical Adhesive 68, Thorlabs) exposed to UV light for 60 seconds. The presence of glue can slightly affect the effective thickness of the cell.

We use the liquid crystal 5CB (4-cyano-4'-pentylbiphenyl, Kingston Chemicals), which has a nematic phase around room temperature ($18° − 35°C$). For the purpose of this work, the chiral dopant COC (Cholesteryl oleyl carbonate, Sigma-Aldrich) is added to twist the nematic director. COC weight concentration varies in each batch depending on the required pitch length according to the relation $c = 1/(p \cdot HTP)$, where p is the pitch and HTP is the helical twisting power. In the case of COC, $HTP = 2.817\mu m^{-1}$[38], as we experimentally verified in a Cano-
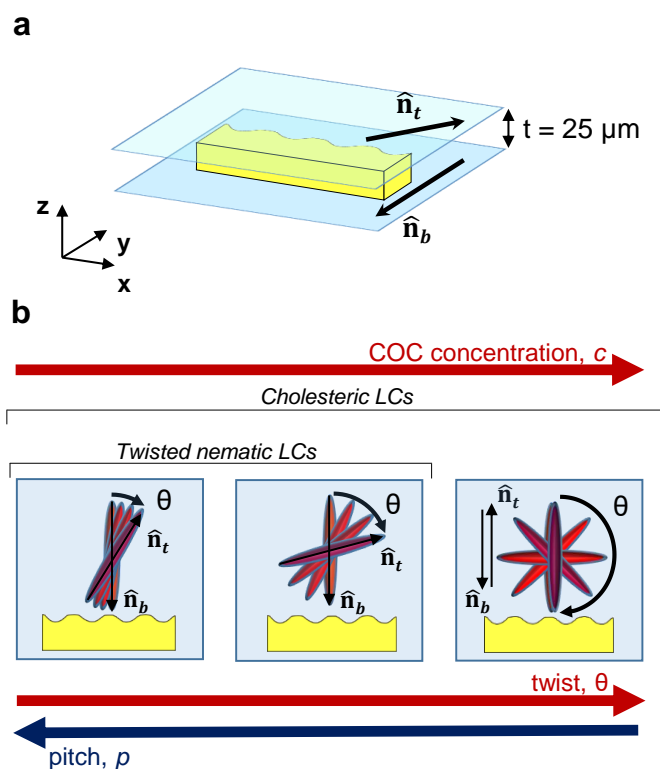
Fig. 1 a) Schematic of the experimental setup. The vessel is delimited by two glass slides with uniform planar anchoring $\hat{n}_t$ at the top and $\hat{n}_b$ at the bottom. The two anchoring directions form an angle θ, which corresponds to the desired twist. A SU-8 wavy wall acts as a vertical spacer (thickness $t = 25\mu$m) and as vertical boundaries. b) Schematic of the experimental cells. The angle θ is increased in order to explore particle behaviors at different twists. For $\theta < \pi/2$ twist can be given by boundaries (twisted nematic LCs) or by chiral dopant COC at a proper concentration c (cholesteric LCs). For larger twists ($\theta > \pi/2$) a purely geometric constraint is not sufficient.

Granjean cell[39].

Table 1 Experimental parameters in different cell configurations used in this work.

Sample	c (% COC)	p (μm)	θ (°)
1[30]	0	∞	0
2	0.1	355	25
3	0.3	118.3	75
4	0.7	50	180

Silica particles (diameter $2a = 15\mu$m unless noted otherwise, Corpuscular Inc.) treated with DMOAP are dispersed in the liquid crystal. The colloidal suspension is injected in the cell while in the isotropic phase ($T \sim 45°C$) and then quenched at room temperature. All the colloids tend to levitate around the mid-cell due to the elastic repulsion from the top and bottom boundaries[40,41]. The sample is observed under optical microscopy (Zeiss AxioImager M1m) in transmitted mode with a 50X objective. All the images and videos are acquired by a high-resolution camera (Zeiss AxioCam HRc) (pixel size: 0.312 μm). Due to the slow dynamics of colloidal particles in the highly-viscous liquid crystalline phase, the typical frame-rate for video acquisition is 1 frame/min;

all ESI†Videos are reported at an accelerated frame rate (180x). In order to add a driving force in the system, the cell is tilted by an angle $\alpha = 0.04$ rad. The force acting on the particle is $\mathbf{F}_g = m\mathbf{g}\sin\alpha$, where m is the particle mass and $\mathbf{g}$ is gravity acceleration. The force is perpendicular to the wall to direct particle motion toward or away from it and to probe for attraction/repulsion in its vicinity. We have verified that far from the wall the tilted cell induced a motion at constant velocity due to the balance between the driving force and the viscous drag[31]. Numerical simulations consist of a relaxation scheme for the Landau-de Gennes free energy, in terms of the $\mathbf{Q}$-tensor order parameter, using a finite difference approach on a cubic grid[42]. Simulations yield the 3-D director field that minimizes Landau-de Gennes (LdG) free energy. Convergence is determined by small relative change in $\mathbf{Q}$, lower than 10^{-3}. We note the usual caveats in comparing any simulated liquid crystalline energy landscape, which include: (i) the inability to rescale all lengths from the experiment equally in the simulation, since the mesh size cannot exceed the defect core size set by the nematic correlation length, which therefore cannot be "scaled out" of the problem, and which is thousands of times smaller than the particle size in experiment; (ii) the prohibitive cost to simulating microscale particles; (iii) the differing stable defect configurations with particle diameter, with dipolar type defects being stable for microscale particles, and Saturn rings stable for particles smaller than 300 nm. Because of the different length scales between experiments and simulations, the outcomes cannot replicate exactly the phenomena, but can be used as a guideline for the qualitative features of the free energy landscape and director fields[18,20,26,31,42,43]. Mesh size is fixed by the correlation length in 5CB (4.5 nm). We rescale all the system dimensions (particle, wall, vessel) in order to keep the same ratio between these sizes. We also impose a stronger anchoring condition than in experiment to ensure $K/W \sim a$ (K is the elastic constant, W is the anchoring strength and a is the particle radius), i.e. anchoring strength is scaled inversely to system size. Typical sizes for the simulation volume are $D_x = 600$ nm (direction parallel to the wall), $D_y = 400$ nm (distance from the wall), $D_z = 400$ nm (vertical direction, thickness of the cell). Particle radius is set at $a = 120$ nm to ensure the same radius-to-thickness ratio as in experiments. Anchoring conditions of any boundary (wall, particle, top and bottom plates) and chirality (via the helical wave number $q_0 = 2\pi/p = \theta/D_z$) are fixed as initial conditions. For most of the applications in this paper, simulations are replicated for different colloid position (x, y, z) in order to map energy landscapes.

3 Results and discussion

3.1 θ-twisted LCs ($0 < \theta < \pi/2$)

Starting from the known case of nematic LCs[30] ($\theta = 0$, $p \rightarrow +\infty$, $c = 0$) we follow an incremental approach. We prepare a series of cells with increasing twist θ, i.e. the angle between anchoring directions of top and bottom plates. These cells are filled with both nematic and cholesteric LCs. In the former case, the twisted director field results from frustrations owing to the boundaries. In the latter, the twist is given by the chirality and boundaries accommodate the director field twist along the direction perpen-

dicular to the slides ($\theta/t = 2\pi/p$, where t is the cell thickness and p is the cholesteric pitch). In both cases, the homeotropic anchoring of the wavy wall is arbitrarily chosen to be parallel to the anchoring direction of the bottom plate (Fig. 2a). For gently twisted LCs ($\theta = 25°$, $1°/\mu$m, $p \gg t$, Fig. 2a) no differences in wall-colloid interactions are noticed with respect to the nematic sample[30]. The particles can be divided into different populations according to their defects: Saturn Ring and dipole. Moreover, the companion defect in the dipolar structure can be oriented away from or toward the wall. For a particle with a Saturn ring defect, the splay of the spherical cap is complementary to the splay in the dale, while bend distortions at the ring match with the same ones at the inflection points on the hillsides. Such a particle docks in the dale (Fig. 2b). The same splay-match attraction between dale and spherical surface is observed when the dipole is away from the wall (Fig. 2c). On the contrary, when the interaction is driven by the companion defect it matches with the divergent splay at the hill (Fig. 2d).
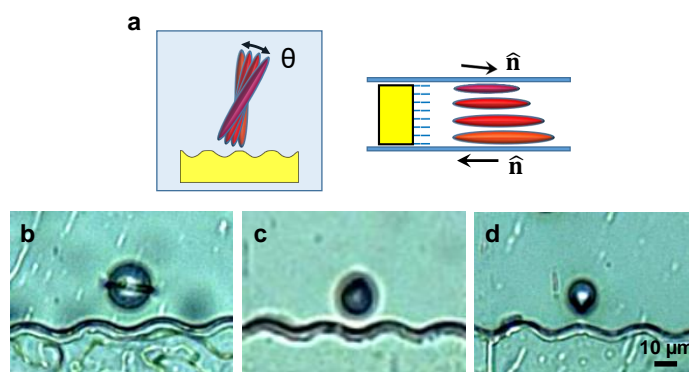

Fig. 2 Homeotropic particles in $25°$-twisted cholesteric liquid crystals in proximity to a wavy wall. a) Scheme of the experimental cell and director field orientation: top view (left) and side view (right). b-d) Final state for homeotropic particles with different defects attracted to the wall: Saturn Ring docking in the dale (b); dipole opposite to wall, docking in the dale (c); dipole oriented towards the wall, attracted at the top of the hill (d).

The only minor difference with respect to nematic LCs is the position of the attractive site in the dale. In nematic LCs the minimum energy configuration is achieved when the particle is centered at the bottom of the dale; in twisted LCs, the attractive site is asymmetrically shifted to the right. Numerical simulations of the director field without a colloid help visualize the reason for this displacement from the dale's center (Fig. 3a). Because of the twist, molecules can better accommodate the homeotropic anchoring condition on the left side of the dale. For similar reasons, a strong bend distortion (yellow highlight) is needed on the right side. The presence of a colloid here removes the highest energy density region and interacts compatibly with the local director field, resulting in the most favorable attraction site. In this case, the energy landscape is not affected by the source of twist. The same particle behavior is observed for twisted nematic and cholesteric LCs. We simulate a homeotropic colloid close to the wavy wall. The anchoring directions of the top and bottom boundaries of the simulation volume form an angle $\theta = 25°$, as in the samples used in experiments. We change the chiral-

ity of the liquid crystal phase. We use three different values for the helical wave number $q_0 = 2\pi/p$: 0 (this corresponds to nematic LCs, in which the twist is induced only by frustration from the confinement), $0.5 \cdot 10^{-3}$ nm^{-1} (long-pitch cholesteric LCs, twist is given by both frustration and chirality), $1.0 \cdot 10^{-3}$ nm^{-1} (cholesteric LCs). In the latter, the twist induced by chirality corresponds exactly to $\theta = 25°$ over the cell thickness. In this case, boundaries accommodate, but do not frustrate, the twist. All three systems give, within few $k_B T$s, the same energy difference $\Delta E(x,y) = E(x,y) - E_0$, where E_0 is the far field energy (Fig. 3b). We can state that energy gradients (and so, trajectories and equilibrium locations) depend only on twist angle θ but not on chiral dopant concentration c. The presence of chiral dopant has effect only on lowering the absolute value of the elastic energy (Fig. 3c).
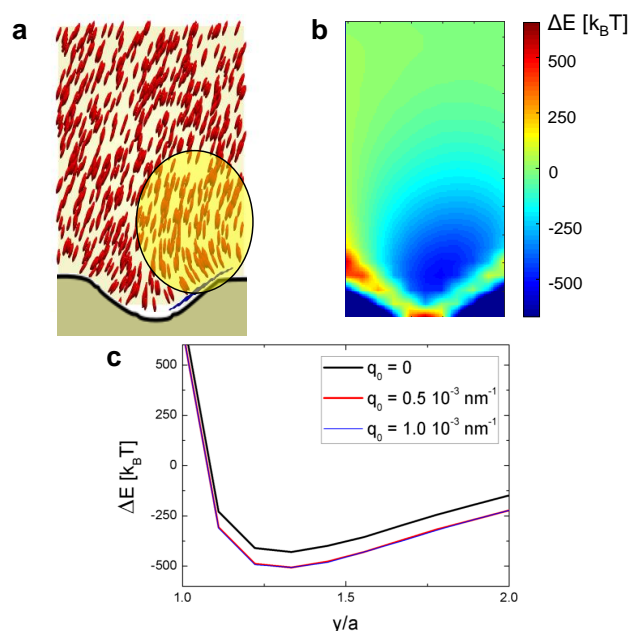
Fig. 3 Simulations in $25°$-twisted cell. a) Simulated molecular orientation at a plane $z = t/2$ in proximity of a dale, without colloids. The highlighted region indicates the maximum bend distortion. b) 2-D color map of the energy landscape ΔE as a function of the particle position in proximity of the wall. $\Delta E = E - E_0$, where E_0 is the far field energy. The same $\Delta E(x,y)$ within few $k_B T$s is obtained for twisted nematic ($q_0 = 0$), partially doped cholesteric ($q_0 = 0.5 \cdot 10^{-3}$ nm^{-1}), cholesteric ($q_0 = 1.0 \cdot 10^{-3}$ nm^{-1}) LCs. c) Energy vs. normalized distance y/a (a radius of the particle) for a colloid in the mid-cell ($z = t/2$) and centered on the wall ($x = 0$). For nematic LCs ($q_0 = 0$, black line) the curve is shifted toward small absolute energy value. For cholesteric LCs ($q_0 = 0.5 \cdot 10^{-3}$ nm^{-1}, $1.0 \cdot 10^{-3}$ nm^{-1}, red and blue lines) the curves are superposed.

The twist is increased up to $\theta = 75°$. The corresponding pitch is $p = 113.5 \mu$m $> t$, corresponding to a chiral dopant concentration $c = 0.3\%$. Most of the particles show a curled dipole defect (Fig. 4), in agreement with the literature[44]. Unlike the previous case in which dipoles oriented toward the wall were attracted by the hill, the presence of a large twist causes these colloids to remain a few radii away from the boundary surface. Colloids several radii from the wall approach it only under the action of an external driving force $\mathbf{F}_g$. In the vicinity of the wall, the repulsive elastic

potential repels them. The particles stop at an equilibrium site determined by the balance between these forces (Fig. 4a-c, and ESI†Video S1). Colloids initially forced to be closer to the hill are repelled. In this case (Fig. 4d-f, and ESI†Video S2) the cell is not tilted, so there is no external force to drive the particle toward the wall. The purely repulsive potential pushes the particle away from the wall to a distance at which the repulsive force becomes negligible. This location indicates the decay length of this repulsive interaction.
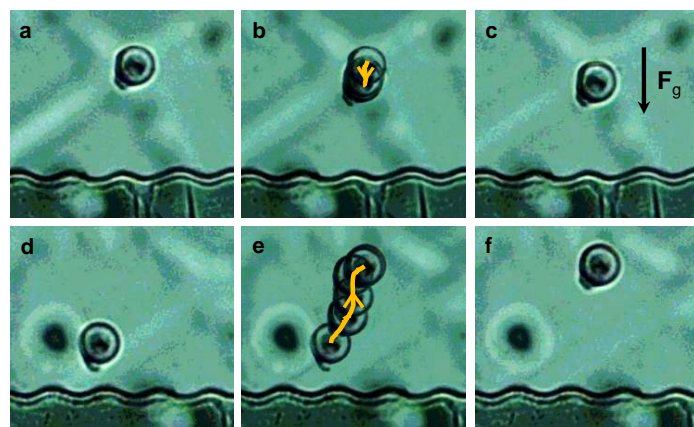
Fig. 4 Particles with a curled dipole in $75°$-twisted cholesteric liquid crystals. a-c) Initial state (a), time-stack visualization (frame rate: 1 image/min) of the trajectory (b) and final state (c) of a particle in the far field under the action of a driving force directed toward the wall. The particle approaches the top of the hill up to the equilibrium site in (c), given by the balance of elastic and driving forces, and stays there until the end of the acquisition. d-f) Initial state (d), time-stack visualization (frame rate: 1 image/min) of the trajectory (e) and final state (f) of a particle starting in close proximity to the wall (no external force involved here). The particle is initially repelled from the wall until the repulsive gradient becomes negligible.

Under stronger confinement it is possible to stabilize more twisted loop defects winding around the colloid[43,45,46]. This goal is achieved by using larger particle diameters ($2a = 18 \mu$m), i.e. larger a/t ratio, and stronger anchoring conditions at the boundaries. In this case, both glass plates (top and bottom boundaries) are coated with polyimide instead of PVA. Sample preparation follows the same protocol as in the previous cases. Positive energy gradients along a distance of the order of few particle diameters are observed when the particle is directed toward the wall. In Fig. 5a-b a homeotropic particle shows a distorted loop defect (inset), whose orientation and position are determined by the twist distortion of the hosting LCs phase. In Fig. 5a, and ESI†Video S3 the colloid approaches the wall due to the external driving force $\mathbf{F}_g$, and then stops at a free energy minimum. The same particle is still able to move (Fig. 5b, and ESI†Video S4) parallel to the wall, confirming empirically our hypothesis. A further confirmation comes from numerical simulations (Fig. 5d). Simulated particles show the characteristic twisted loop defect (inset). We computed the free energy of the system for different particle positions in the plane (x,y) at the mid-cell ($z = t/2$). False color map shows $\Delta E = E - E_0$, where E_0 denotes the energy in the bulk, far from any boundary. The wall dales are still regions of attraction

(light blue), and hills remain region of repulsion (red). However, an energy gradient (yellow region near the dashed line) appears because of the large twist, arresting particle dynamics.
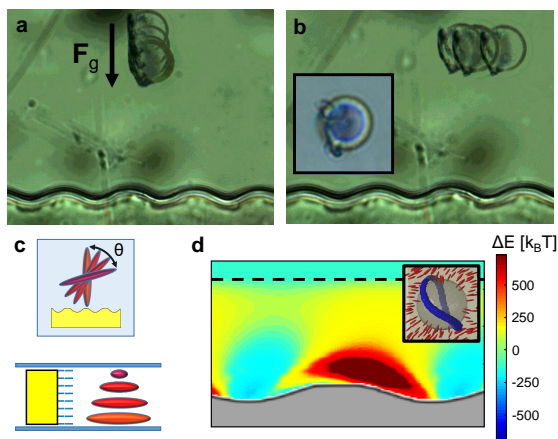
Fig. 5 Homeotropic particle with a twisted loop defect in $75°$-twisted cholesteric liquid crystals in a vessel with strong planar anchoring. a) Time-stack visualization (frame rate: 1 image/min) of the trajectory of a particle under the effect of an external driving force $\mathbf{F}_g$. The particle stops at an equilibrium site determined by the balance between driving and elastic forces. b) Time-stack visualization (frame rate: 1 image/min) of the same particle in (a) after approach. The particle is able to move because of diffusion and internal drift (no pinning at the boundary), but keeping the same distance from the wall. Inset: snapshot of the particle under crossed-polarizers, showing the twisted loop. c) Scheme of the experimental setup. Top view (top) shows the twist of the director field by an angle θ along the vertical axis. Side view (bottom) shows the director field orientation at the homeotropic wall and in the far field. d) 2-D color map of the energy landscape ΔE as a function of the particle position. Inset: twisted loop defect around a particle, resulting from numerical simulations.

3.2 π-twisted LCs

At $c = 0.7\%$ COC the cholesteric pitch is $p = 50\mu m$, i.e. twice the cell thickness. The director field undergoes a π-rotation in the sample. The uniform planar anchoring conditions at the top and bottom glass slides have the same direction. Anti-parallel alignment is chosen in order to minimize the splay induced by pre-tilt anchoring at the boundaries, but is irrelevant for the director field twist ($\hat{\mathbf{n}} \equiv -\hat{\mathbf{n}}$). We choose two characteristic configurations for the wall orientation with respect to anchoring alignment of the glass slides: molecular anchoring at the wall parallel (Fig. 6a) or perpendicular (Fig. 6e) to molecular anchoring at the glass plates.

In the parallel configuration (Fig. 6b-d, and ESI†Video S5) the colloids tend to occupy the mid-cell region corresponding to maximum mis-match between wall anchoring and director twist, and so occupy the region with maximum energy cost. Moving always in this horizontal plane, the particles dock in the dale (Fig. 6d). In the perpendicular configuration (Fig. 6f-h, and ESI†Video S6) the maximum mis-match is achieved at the junctions between the boundaries at top and bottom plates ($z = 0$ and $z = t$), but these regions are inaccessible to the colloid for both elastic and steric repulsion. In this system particles do not dock on the wall. Even

if pushed towards the wall by the gravitational driving force $\mathbf{F}_g$ all the colloids stop at an equilibrium distance away from it (Fig. 6h). We used LdG simulation to understand the two different behaviors (Fig. 7). The system energy is computed for parallel and perpendicular alignments using the same simulation parameters (simulation volume, particle size, boundaries, cholesteric pitch) for both the configurations. The only difference is the orientation of the uniform planar anchoring at the top and bottom boundaries (corresponding to the glass slides in the experimental cell) with respect to the wall. Each computation is repeated placing the particles at different distances from for the wall (x-direction) and positions along the vertical axis (z-direction). For the purpose of this study, the y-position is constant and corresponds to a wall dale. Simulation in parallel alignment (Fig. 7a) confirms a largely attractive potential well in the dale, and a monotonic energy landscape that promotes docking. Simulations in perpendicular alignment (Fig. 7b) show a weaker, but still present, potential well in the dale. However, it is shielded by an energy barrier. For the sake of clarity we extract the representative curves at fixed height (Energy vs. wall distance x at $z = t/2$), as plotted in Fig. 7c. The far field energy is fixed at 0 in both cases. ΔE in parallel configuration (black curve) has a monotonic behavior with minimum at the wall (as in the nematic case). ΔE in perpendicular configuration (red curve) shows a peak of hundreds of $k_B T$ a few radii away from the wall. This barrier is a characteristic signature of the cholesteric liquid crystals with a pitch comparable to the cell size and it does not appear in nematic LC with the same perpendicular anchoring. Its presence is experimentally confirmed by docking of colloids starting close to the wall inside the attractive potential well (ESI†Video S7). Overcoming the barrier by a sufficiently large driving force could allow further mechanisms, as a selective control over particle behavior. Particles could be forced over the barrier by external fields and remained trapped in the well upon removal of that field, an effective "double lock" mechanism.

The different behaviors are understood in the light of the relative alignments of the anchoring of all the boundaries involved, shaping a complex 3-D director field and determining defect loop orientation. For parallel alignment (Fig. 7a) the deep potential well in the dale is given by both splay-matching between the wall and the particle deformations, and removal of a region of high distortion between the wall and the twisted LCs. The defect loop position is compatible with the splay-matching geometry in Fig. 6d. For perpendicular alignment (Fig. 7b) the antagonism between the anchoring imposed by wall (along $\mathbf{y}$), the glass slides (along $\mathbf{x}$) and the particle (on a spherical boundary), combined with the twist of the host phase, creates local traps. Moreover, the defect loop is maximally incompatible to the wall (Fig. 6h) giving overlap between the splay distortion in the dale and the bend distortion at the loop.

The presence and the position of an energy barrier in perpendicular π-twist configuration depend on the particle size-to-thickness ratio. Particles with different diameter $2a$ are tested in the same sample (Fig. 8a-c, and ESI†Video S8). Larger particles ($2a = 18\mu m$) are arrested by an energy barrier a few radii away from the wall, as in the case previously shown in Fig. 6e-h.
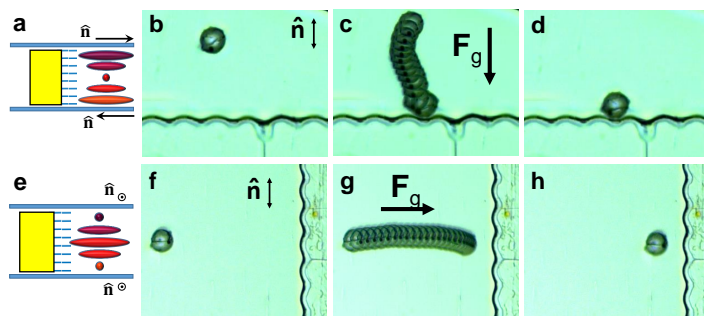
Fig. 6 Colloidal particles in π-twisted cholesteric cells. Figs. a-d refer to the configuration with molecular anchoring at the wall parallel to molecular anchoring at the glass plates. Figs. e-h refer to the configuration with molecular anchoring at the wall perpendicular to molecular anchoring at the glass plates. a) Side view scheme of the director field alignment in the cell. b-d) Initial state (b), time-stack visualization (frame rate: 1 image/min) of the trajectory (c) and final state (d) of homeotropic particles docking in the dales. e) Side view scheme of the director field alignment in the cell. f-h) Initial state (f), time-stack visualization (frame rate: 1 image/min) of the trajectory (g) and final state (h) of homeotropic particles approaching the wall under the action of an external driving force. The particles stop away from the wall without docking.
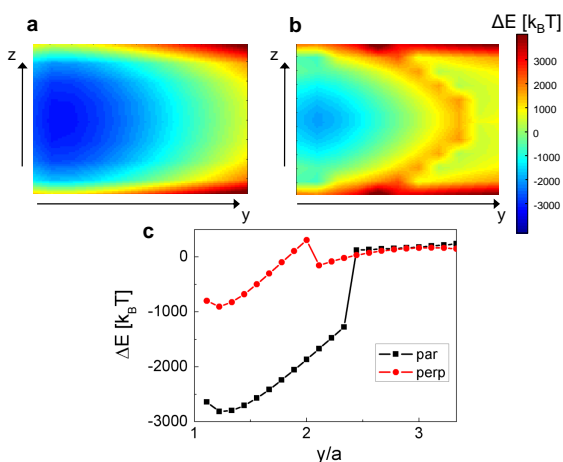
Fig. 7 Numerical simulation of homeotropic colloids winded by twisted loop defects in the π-twisted cell. a) 2-D map of a particle centered on the dale as a function of the vertical position z and distance from the wall y for configuration 1. b) 2-D map of a particle centered on the dale as a function of the vertical position z and distance from the wall y for configuration 2. c) Comparison of the energies in the two cases, at fixed height ($z = t/2$). Particle in configuration 1 (black curve) docks in the dale. Colloid in configuration 2 (red curve) is stopped by a barrier around $y = 2a$.

Smaller particles ($2a = 12\mu$m), on the contrary, dock in the dale. Very small particles ($2a = 2.12\mu$m) find no energy barrier and are attracted to the wall (Fig. 8d). However, since there is no splay matching between particle and wall dales, any position along the wall contour is a suitable attraction site (Fig. 8e). Moreover, since a disclination line is present at the wall boundary (Fig. 8f), it contributes to irreversibly trap the particle. Defect position and orientation have a role in size-dependent behavior. When $2a \sim t$, strong confinement determines an antagonist defect orientation, for both twisted loops and dipoles, with respect to the wall. When

the colloid size compared to the cell thickness is smaller, defects are not as constrained by boundaries. Defects can slightly rotate and adjust to a configuration compatible with the colloid being nearly in contact with the wall, as observed by the re-alignment of the dipole of the smaller particle in Figs. 8a-c.
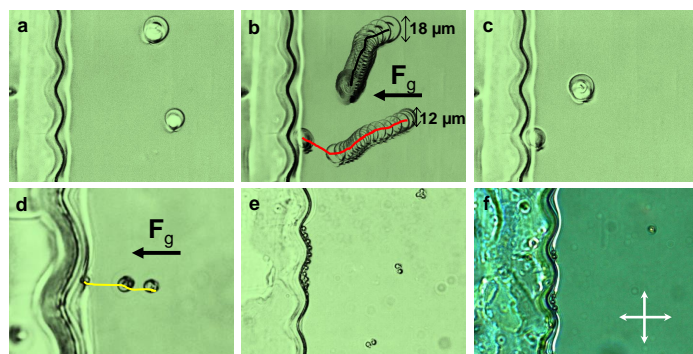
Fig. 8 Size effect of particle interaction in π-twisted cholesteric cells with perpendicular anchoring alignment. a-c) Two particles with different diameters are observed in the same sample: initial state (a), time-stack visualization (frame rate: 1 image/min) of the trajectories (b), final state (c). The larger particle ($2a = 18\mu$m, black trajectory) fluctuates at an equilibrium distance from the wall. The smaller particle ($2a = 12\mu$m, red trajectory) does not find any barrier and dock in the dale, trapped in a disclination line. It is possible to see the particle acceleration in proximity of the wall. d) Wall-particle attraction a particle of size $2a = 2.12\mu$m. e) Accumulation of small particles along the wall contour, where any point is a suitable attraction site. f) Crossed polarized image of a disclination line at the wall boundary, trapping the particle irreversibly.

4   Conclusions

We studied particle interactions with an undulated wall in a confined cell in the presence of twisted nematic and cholesteric liquid crystals. While in untwisted nematics LCs the particle dynamics are driven by splay and bend distortions, in these new systems twist deformations assume a key role. In particular, twist introduces a new length scale, the pitch p, in addition to other sample parameters (particle diameter, cell thickness, wavy wall wavelength and radius of curvature). This results in an adjustable wall-colloid interaction, where docking can occur only in a range of pitch or in peculiar anchoring. This behavior can pave the way to a switchable adsorption of colloids mediated by external stimuli able to adjust the twist. A tool is this direction can be provided, for instance, by pitch phototuning[47] or by photosensitive anchoring controlled by polarized light[22,37,48,49].

Conflicts of interest

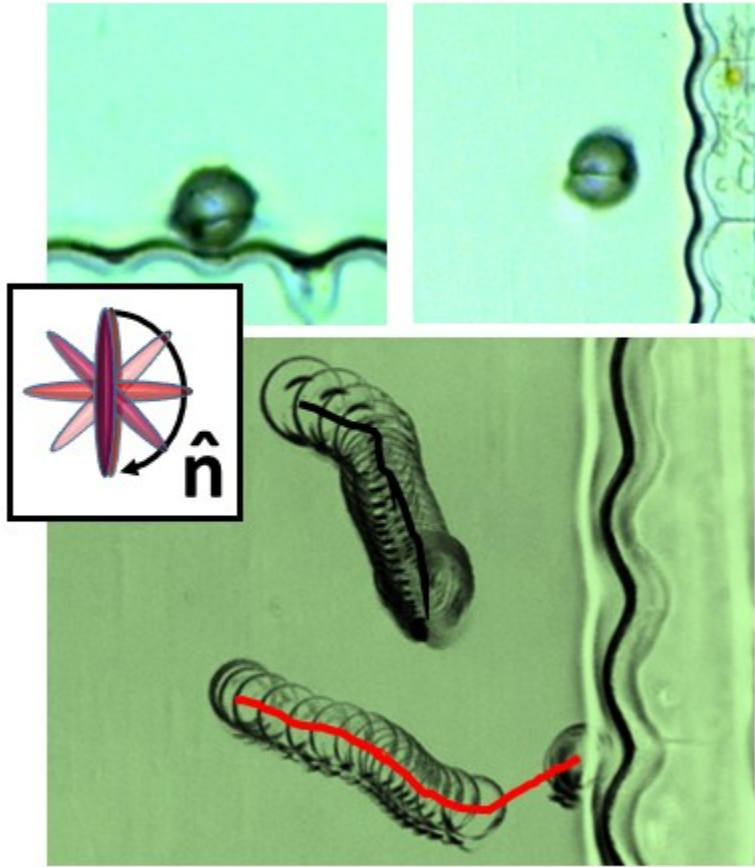The authors declare no competing financial interest.

Acknowledgements

Notes and references

1 G. M. Whitesides and B. Grzybowski, *Science*, 2002, **295**, 2418–2421.

2 S. C. Glotzer, M. J. Solomon and N. A. Kotov, *AIChE J.*, 2004, **50**, 2978–2985.

3 V. N. Manoharan, *Science*, 2015, **349**, 1253751.

4 M. Wang, L. He, W. Xu, X. Wang and Y. Yin, *Angew. Chem. Int. Ed.*, 2015, **54**, 7077–7081.

5 N. Vogel, S. Utech, G. T. England, T. Shirman, K. R. Phillips, N. Koay, I. B. Burgess, M. Kolle, D. A. Weitz and J. Aizenberg, *Proc. Natl. Acad. Sci.*, 2015, **112**, 10845–10850.

6 A. S. J. Iyer and L. A. Lyon, *Angew. Chem. Int. Ed.*, 2009, **48**, 4562–4566.

7 M. Diba, H. Wang, T. E. Kodger, S. Parsa and S. C. G. Leeuwenburgh, *Adv. Mater.*, 2017, **29**, 1604672.

8 S. Sivakumar, K. L. Wark, J. K. Gupta, N. L. Abbott and F. Caruso, *Adv. Funct. Mater.*, 2009, **19**, 2260–2265.

9 P. Di Palma, C. Taddei, A. Borriello, G. De Luca, M. Giordano, A. Iadicicco, S. Campopiano and L. Sansone, *IEEE Photon. J.*, 2017, **9**, 1–11.

10 Y. Zhao and T. Ikeda, *Smart light-responsive materials: azobenzene-containing polymers and liquid crystals*, John Wiley & Sons, 2009.

11 B. Bharti and O. D. Velev, *Langmuir*, 2015, **31**, 7897–7908.

12 M. J. Solomon, *Langmuir*, 2018, **34**, 11205–11219.

13 C. Blanc, D. Coursault and E. Lacaze, *Liq. Cryst. Rev.*, 2013, **1**, 83–109.

14 D. Pires, J.-B. Fleury and Y. Galerne, *Phys. Rev. Lett.*, 2007, **98**, 247801.

15 F. C. Frank, *Discuss. Faraday Soc.*, 1958, **25**, 19–28.

16 P. G. De Gennes and J. Prost, *The Physics of Liquid Crystals*, Oxford University Press, 2nd edn, 1995, vol. 83.

17 M. Kleman and O. D. Lavrentovich, *Philos. Mag.*, 2006, **86**, 4117–4137.

18 A. Nych, U. Ognysta, M. Škarabot, M. Ravnik, S. Žumer and I. Muševič, *Nat. Commun.*, 2013, **4**, 1489.

19 B. Senyuk, Q. Liu, E. Bililign, P. D. Nystrom and I. I. Smalyukh, *Phys. Rev. E*, 2015, **91**, 040501.

20 I. Muševič, M. Škarabot, U. Tkalec, M. Ravnik and S. Žumer, *Science*, 2006, **313**, 954–958.

21 J. C. Loudet, P. Barois, P. Auroy, P. Keller, H. Richard and P. Poulin, *Langmuir*, 2004, **20**, 11336–11347.

22 A. Martinez, H. C. Mireles and I. I. Smalyukh, *Proc. Natl. Acad. Sci.*, 2011, **108**, 20891–20896.

23 C. Peng, T. Turiv, Y. Guo, S. V. Shiyanovskii, Q.-H. Wei and O. D. Lavrentovich, *Sci. Adv.*, 2016, **2**, e1600932.

24 H. Yoshida, K. Asakura, J. Fukuda and M. Ozaki, *Nat. Commun.*, 2015, **6**, 7180.

25 N. M. Silvestre, P. Patricio and M. M. Telo da Gama, *Phys. Rev. E*, 2004, **69**, 061402.

26 Y. Luo, F. Serra, D. A. Beller, M. A. Gharbi, N. Li, S. Yang, R. D. Kamien and K. J. Stebe, *Phys. Rev. E*, 2016, **93**, 032705.

27 F. Serra, *Liq. Cryst.*, 2016, **43**, 1920–1936.

28 N. M. Silvestre, Q. Liu, B. Senyuk, I. I. Smalyukh and M. Tasinkevych, *Phys. Rev. Lett.*, 2014, **112**, 225501.

29 X. Li, J. C. Armas-Pérez, J. P. Hernández-Ortiz, C. G. Arges, X. Liu, J. A. Martínez-González, L. E. Ocola, C. Bishop, H. Xie, J. J. de Pablo and P. F. Nealey, *ACS nano*, 2017, **11**, 6492–6501.

30 Y. Luo, F. Serra and K. J. Stebe, *Soft Matter*, 2016, **12**, 6027–6032.

31 Y. Luo, D. A. Beller, G. Boniello, F. Serra and K. J. Stebe, *Nat. Commun.*, 2018, **9**, 3841.

32 H. Finkelmann and H. Stegemeyer, *Ber. Bunsenges. Phys. Chem.*, 1978, **82**, 1302–1308.

33 H. Kimura, M. Hosino and H. Nakano, *J. Phys. Colloq.*, 1979, **40**, C3–174.

34 T. Sagisaka and Y. Yokoyama, *Bull. Chem. Soc. Jpn.*, 2000, **73**, 191–196.

35 J. Jiang and D.-K. Yang, *Phys. Rev. Appl.*, 2017, **7**, 014014.

36 P. Oswald, A. Dequidt and A. Żywociński, *Phys. Rev. E*, 2008, **77**, 061703.

37 R. F. de Souza, E. K. Lenzi, R. T. de Souza, L. R. Evangelista, Q. Li and R. S. Zola, *Soft Matter*, 2018, **14**, 2084–2093.

38 N. I. Lebovka, L. N. Lisetski, M. I. Nesterenko, V. D. Panikarskaya, N. A. Kasian, S. S. Minenko and M. S. Soskin, *Liq. Cryst.*, 2013, **40**, 968–975.

39 P. Oswald and P. Pieranski, *Nematic and cholesteric liquid crystals*, Taylor & Francis, 1st edn, 2005.

40 O. D. Lavrentovich, *Soft Matter*, 2014, **10**, 1264–1283.

41 O. P. Pishnyak, S. Tang, J. R. Kelly, S. V. Shiyanovskii and O. D. Lavrentovich, *Phys. Rev. Lett.*, 2007, **99**, 127802.

42 M. Ravnik and S. Žumer, *Liq. Cryst.*, 2009, **36**, 1201–1214.

43 V. S. R. Jampani, M. Škarabot, M. Ravnik, S. Čopar, S. Žumer and I. Muševič, *Phys. Rev. E*, 2011, **84**, 031703.

44 Y. Tong, Y. Wang and P. Zhang, *Numer. Math.-Theory Me.*, 2017, **10**, 205–221.

45 J. S. Lintuvuori, D. Marenduzzo, K. Stratford and M. E. Cates, *J. Mater. Chem.*, 2010, **20**, 10547–10552.

46 J. S. Lintuvuori, K. Stratford, M. E. Cates and D. Marenduzzo, *Phys. Rev. Lett.*, 2010, **105**, 178302.

47 A. Bosco, M. G. M. Jongejan, R. Eelkema, N. Katsonis, E. Lacaze, A. Ferrarini and B. L. Feringa, *J. Am. Chem. Soc.*, 2008, **130**, 14615–14624.

48 G. Fang, Y. Shi, J. E. Maclennan, N. A. Clark, M. J. Farrow and D. M. Walba, *Langmuir*, 2010, **26**, 17482–17488.

49 Y. Shi, G. Fang, M. A. Glaser, J. E. Maclennan, E. Korblova, D. M. Walba and N. A. Clark, *Langmuir*, 2014, **30**, 9560–9566.

111x121mm (96 x 96 DPI)